Since January 2020 Elsevier has created a COVID-19 resource centre with free information in English and Mandarin on the novel coronavirus COVID-19. The COVID-19 resource centre is hosted on Elsevier Connect, the company's public news and information website.

Phytochemistry 212 (2023) 113713

Contents lists available at ScienceDirect

Phytochemistry

journal homepage: www.elsevier.com/locate/phytochem

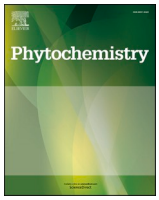

Cruciferous vegetable-derived indole-3-carbinol prevents coronavirus cell egression mechanisms in tracheal and intestinal 3D *in vitro* models.

Georgia Pennarossa [a], Sharon Arcuri [a], Rolando Pasquariello [b], Fulvio Gandolfi [b], Margherita Maranesi [c,*], Tiziana A.L. Brevini [a,**]

[a] *Laboratory of Biomedical Embryology and Tissue Engineering, Department of Veterinary Medicine and Animal Sciences, Università Degli Studi di Milano, Via Dell'Università 6, 26900, Lodi, Italy*
[b] *Department of Agricultural and Environmental Sciences - Production, Landscape, Agroenergy, Università Degli Studi di Milano, Via Celoria 10, 20133, Milan, Italy*
[c] *Department of Veterinary Medicine, University of Perugia, Via S. Costanzo 4, 06126, Perugia, Italy*

ARTICLE INFO

Keywords:
3D *in vitro* models
Coronavirus
Cruciferous
Indole-3-carbinol
Intestine
Trachea

ABSTRACT

The potential antiviral effects of indole-3-carbinol (I3C), a phytochemical found in *Cruciferous* vegetables, were investigated. Fibroblasts and epithelial cells were co-cultured on Alvetex® scaffolds, to obtain *ad hoc* 3D *in vitro* platforms able to mimic the trachea and intestinal mucosae, which represent the primary structures involved in the coronavirus pathogenesis. The two barriers generated *in vitro* were treated with various concentrations of I3C for different incubation periods. A protective effect of I3C on both intestinal and trachea models was demonstrated. A significant reduction in the transcription of the two main genes belonging to the Homologous to E6AP C-terminus (HECT)-E3 ligase family members, namely NEDD4 E3 Ubiquitin Protein Ligase (NEDD4) and WW Domain Containing E3 Ubiquitin Protein Ligase 1 (WWP1), which promote virus matrix protein ubiquitination and inhibit viral egression, were detected.

These findings indicate I3C potential effect in preventing coronavirus cell egression processes that inhibit viral production. Although further studies are needed to clarify the molecular mechanisms whereby HECT family members control virus life cycle, this work paves the way to the possible therapeutic use of new natural compounds that may reduce the clinical severity of future pandemics.

1. Introduction

Indole-3-carbinol (I3C; C9H9NO) is a plant-derived phytochemical found in the family *Brassicaceae*, also known as Cruciferous vegetables, that includes broccoli, cabbage, cauliflower, brussels sprouts, and daikon (Takada et al., 2005). I3C derives from the breakdown of the glucosinolate glucobrassicin, by the enzymatic activity of the myrosinase (β-thioglucosidase) that catalyzes the hydrolysis of glucosinolates in intact plant cells (Zhao et al., 2015). In addition, when plant cells are damaged or disrupted through chewing or chopping, glucobrassicin is exposed to the enzyme myrosinase that hydrolyzes it to a glucose molecule and an unstable aglycone intermediate, thiohydroxanate-O-sulfate, which is then continuously converted into different classes of breakdown products (Singh et al., 2021a). More in detail, further catalysis of it results in the formation of 3-indolylmethylisothiocyanate that readily converts to a thiocyanate ion and I3C (Kim et al., 2008). Glucosinolate breakdown products are generally implicated in human health, and I3C has been shown to display prophylactic potential against several conditions (Singh et al., 2021b). For instance, it was reported to have antibacterial and antifungal activities against human pathogenic microorganisms (Sung and Lee, 2007), as well as antioxidant properties (Singh et al., 2021b) and cancer-preventive effects (Weng et al., 2008). The mechanism by which I3C mediates these processes still remain unclear, although a direct involvement of a variety of signaling pathways has been suggested (Li et al., 2003).

Here, the potential antiviral effect of I3C and its ability to inhibit viral egression are investigated. To this purpose, *ad hoc* 3D platforms that recapitulate *in vitro* the tracheal and intestinal mucosa structures - which represent the primary targets of the coronavirus infection (Gavriatopoulou et al., 2020; Troisi et al., 2021) - are developed. Specifically, fibroblasts and epithelial cells are co-cultured on Alvetex® scaffold inserts and the generated model ability to closely mimic the complex

* Corresponding author.
** Corresponding author.
E-mail addresses: margherita.maranesi@unipg.it (M. Maranesi), tiziana.brevini@unimi.it (T.A.L. Brevini).

https://doi.org/10.1016/j.phytochem.2023.113713
Received 21 December 2022; Received in revised form 4 May 2023; Accepted 5 May 2023
Available online 9 May 2023

morphological and functional features of two epithelial barriers is investigated, through histological and molecular analyses. Subsequently, various doses of I3C for different incubation periods are tested to evaluate the phytochemical ability to inhibit viral egression. The results obtained demonstrate a protective effect of the nutraceutical on both intestinal and trachea models. In particular, it is detected a significantly reduced transcription of the two main genes belonging to the Homologous to E6AP C-terminus (HECT)-E3 ligase family, namely NEDD4 E3 Ubiquitin Protein Ligase (NEDD4) and WW Domain Containing E3 Ubiquitin Protein Ligase 1 (WWP1), which are known to be able to promote virus matrix protein ubiquitination and to inhibit viral egression (Novelli et al., 2021), thus possibly decreasing viral production.

2. Results and discussion

2.1. Development of ad hoc 3D culture in vitro models and validation

2.1.1. Porcine intestinal 3D culture model assembly

The normal porcine enterocyte cell line IPEC-J2 cells represents a well-established *in vitro* model to study intestinal physiology, because of its ease of culture as well as its spontaneous differentiation ability (Pi et al., 2022). In addition, this cell line is neither transformed nor tumorigenic in nature and more closely mimics human intestinal physiology than any other cell line of non-human origin (Vergauwen, 2015). Despite these relevant advantages, when IPEC-J2 cells are grown in bidimensional (2D) culture systems, they form monolayers, exhibit highly unphysiological trans-epithelial electrical resistance (TEER) values and low permeability, lacking the morphological and functional complexity of the *in vivo* native tissue.

During the last years, several advances have been made to overcome these limitations, through the use of alternative culture substrates or increasing model complexity in an attempt to obtain more realistic TEER and permeability values (Antunes et al., 2013; Béduneau et al., 2014; Matsusaki et al., 2015; Pereira et al., 2015; Schweinlin et al., 2016; Takenaka et al., 2014). Nevertheless, such systems lack endogenous molecules and interactions and fail to account for the spatial organization distinctive of the mucosal tissue, due to the absence of the stromal compartment (Matsusaki et al., 2015). Consistent with this hypothesis, several evidence demonstrated that intestinal epithelial structure and function are strongly influenced by cell-to-cell and cell-to- extracellular matrix (ECM) interactions (Bernardo and Fibbe, 2013; Halttunen et al., 1996; Kedinger et al., 1998). Indeed, although fibroblast secretome remains largely unknown, the secreted peptides and ECM components have been shown to enhance epithelial morphology and function in a variety of tissues (Halttunen et al., 1996; Hausmann et al., 2019; Korpos et al., 2010). With this in mind, in this manuscript, we co-culture stromal (Fig. 1 A) and epithelial cells (Fig. 1 B) to create a 3D intestinal model

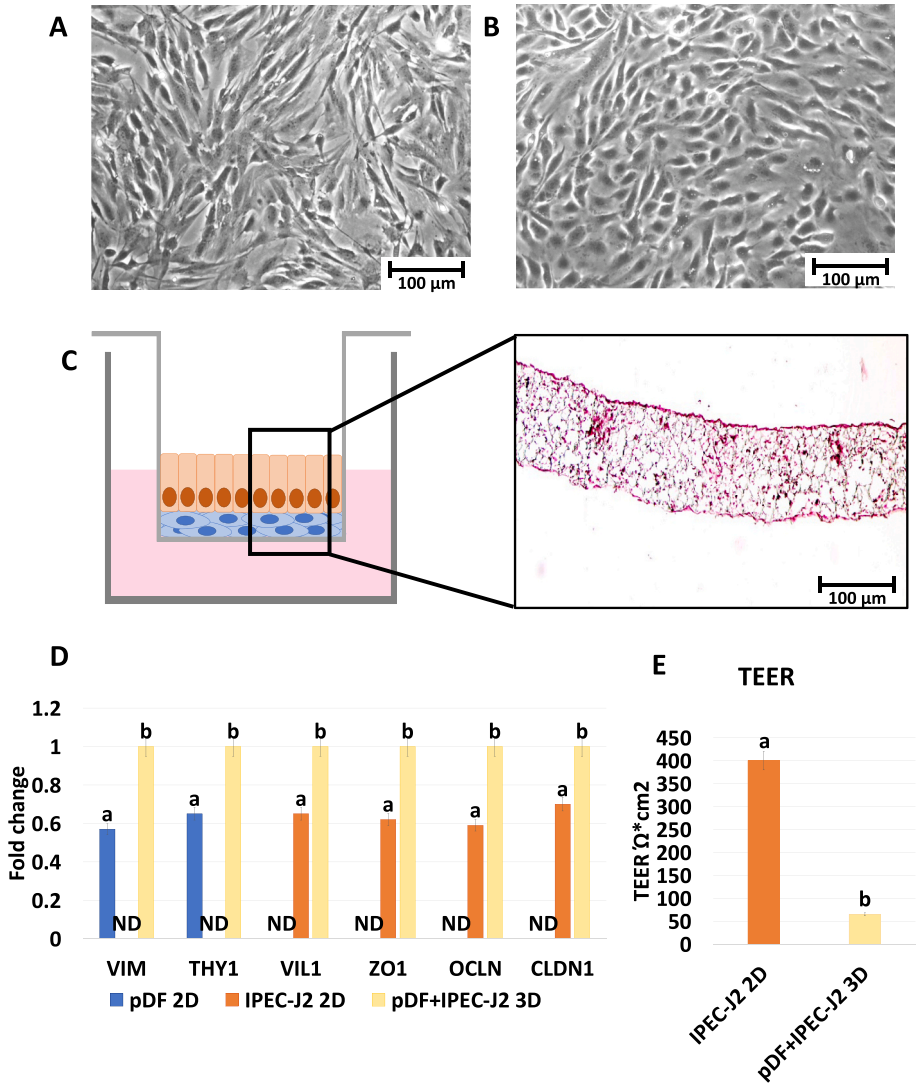

Fig. 1. *Porcine 3D intestinal model generation and validation.* (A) pDF cultured onto 2D standard plastic dishes (scale bar 100 µm). (B) IPEC-J2 cells plated onto 2D standard plastic supports (scale bar 100 µm). (C) Schematic representation of the 3D intestinal model assembled using Alvetex® scaffold inserts and its Haematoxylin and Eosin staining (scale bar 100 µm). (D) Gene expression levels of VIM, THY1, VIL1, ZO1, OCLN and CLDN genes in pDF culture on 2D culture systems (pDF 2D, blue bars), IPEC-J2 cells plated onto 2D standard plastic supports (IPEC-J2 2D, orange bars) and 3D intestinal model assembled by co-culturing pDF and IPEC-J2 cells onto Alvetex® scaffold inserts (pDF + IPEC-J2 3D, yellow bars). Data are expressed as the mean. Error bars represent the standard error of the mean (SEM). Different superscripts indicate $p < 0.05$. (E) TEER values detected in IPEC-J2 cells plated onto 2D standard plastic supports (IPEC-J2 2D, orange bars) and 3D intestinal model assembled by co-culturing pDF and IPEC-J2 cells onto Alvetex® scaffold inserts (pDF + IPEC-J2 3D, yellow bars). Data are expressed as the mean. Error bars represent the standard error of the mean (SEM). Different superscripts indicate $p < 0.05$. (For interpretation of the references to colour in this figure legend, the reader is referred to the Web version of this article.)

that try to more closely mimic the native tissue. We sequentially seed normal porcine dermal fibroblasts (pDF) onto Alvetex® scaffold inserts and allow cells to infiltrate the membrane for 14 days, using the fibroblast standard culture medium supplemented with TGF β1 and ascorbic acid. This results in the formation of a densely populated fibroblast compartment (Fig. 1 C), ensuring for the creation of a robust structural support that mimics the subepithelial compartment. We are convinced that this step is essential to prevent cells from the epithelial compartment to infiltrate into the porous of the scaffold membrane, as previously described by Darling et al. (2020).

IPEC-J2 cells are then plated onto the 3D stromal compartment and cultured for further 21 days that allow enterocyte differentiation. At the end of the culture period, cells exhibit a distinct polarized morphology with a more elongated columnar shape (Fig. 1 C), distinctive of epithelial cell phenotype. This suggests that the 3D culture system developed is able to induce a better degree of differentiation, generating cells that closely resembles enterocytes *in vivo*. In agreement with the morphological observations, the transcription levels of both the main stromal and epithelial compartment markers, namely VIM, THY1, VIL1, ZO1, OCLN and CLDN, are significantly up regulated in cells grown onto Alvetex® scaffolds compared to those cultured in 2D monolayers (Fig. 1 D). These data are in agreement with previous studies demonstrating a higher ability of the dual compartment model to encourage cell terminal differentiation (Costello et al., 2021; Darling et al., 2020).

Interestingly, histological, and molecular data are further supported by the functional results obtained by TEER analysis. Indeed, the measurements obtained displayed an average of 56.8 ± 6.4 Ω*cm2 (Fig. 1 E) that closely resemble the ones reported for the native tissue *in vivo* (40–60 Ω*cm2) (Richter et al., 2014; Zakrzewski et al., 2013). These findings are consistent with previous studies reporting TEER values similar to human small intestine *in vivo* when Caco-2 cells were co-cultured with fibroblasts onto Alvetex® scaffolds (Darling et al., 2020).

Altogether, we fill that the morphological, molecular, and functional data herein produced indicate the 3D model ability to mimic the intestinal mucosa organization and cell barrier function.

2.1.2. Human tracheal 3D culture model assembly

Based on the results obtained in the porcine intestinal 3D model described in 2.1.1 paragraph demonstrating the influence of subepithelial stromal compartment on epithelial differentiation and functionality, we adopt similar approach and co-culture stromal (Fig. 2 A) and epithelial cells (Fig. 2 B) to generate a tracheal 3D model. We sequentially seed and culture normal human dermal fibroblasts (hDF)

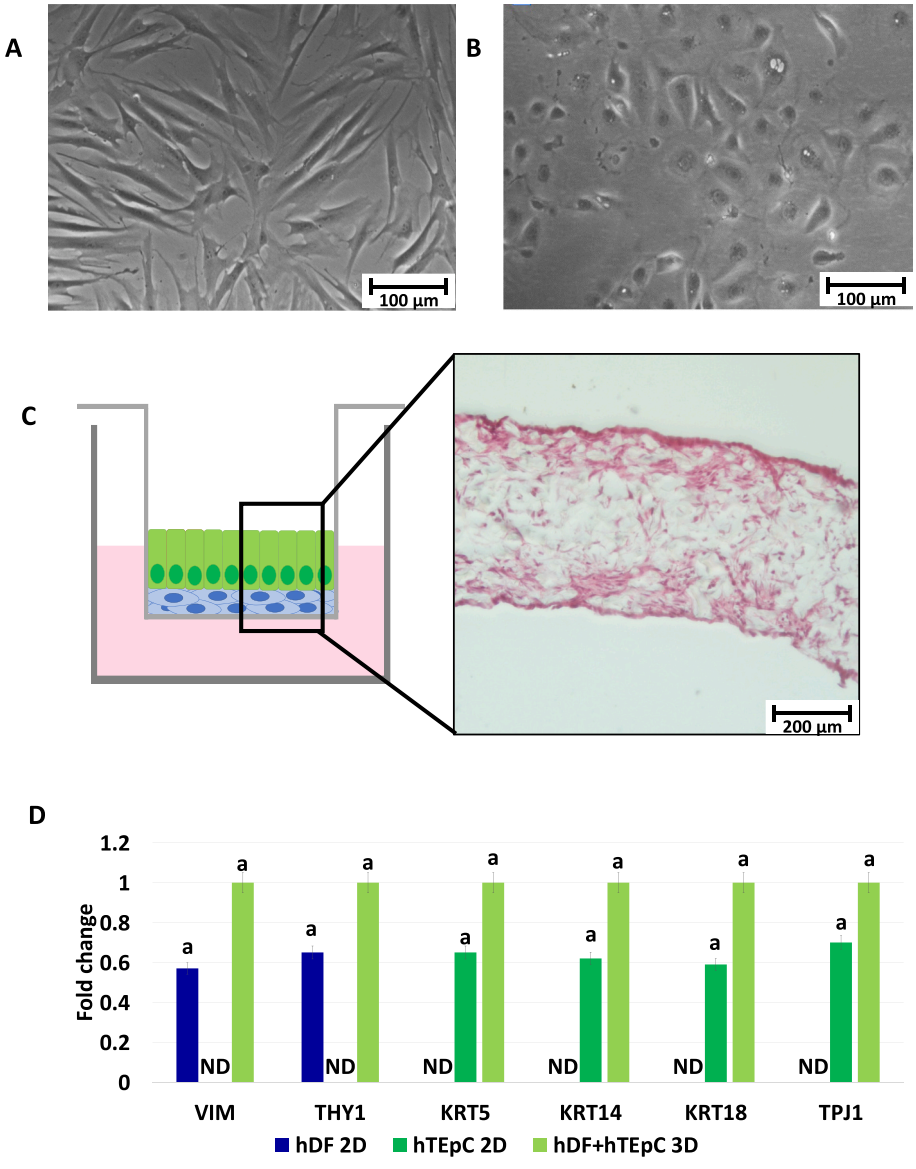

Fig. 2. *Human 3D tracheal model generation and validation.* (A) hDF cultured onto 2D standard plastic dishes (scale bar 100 µm). (B) hTEpC grown onto 2D standard plastic supports (scale bar 100 µm). (C) Schematic representation of the 3D tracheal model assembled using Alvetex® Scaffold inserts and its Haematoxylin and Eosin staining (scale bar 200 µm). (D) Gene expression levels of VIM, THY1, KRT5, KRT14, KRT18, and TJP1 genes in hDF culture on 2D culture systems (hDF 2D, blue bars), hTEpC plated onto 2D standard plastic supports (hTEpC 2D, darl green bars) and 3D tracheal model assembled by co-culturing hDF and hTEpC onto Alvetex® Scaffold inserts (hDF + hTEpC, light green bars). Data are expressed as the mean. Error bars represent the standard error of the mean (SEM). Different superscripts indicate $p < 0.05$. (For interpretation of the references to colour in this figure legend, the reader is referred to the Web version of this article.)

onto Alvetex® scaffolds for 14 days and obtain the formation of a compact and dense stromal compartment (Fig. 2C). Following to the establishment of the subepithelial compartment, normal human tracheal epithelial cells (hTEpC) are plated onto it and cultured for 28 days. At the end of co-culture period, we can observe the presence of a well-formed columnar epithelium similar to the native tracheal mucosa (Fig. 2 C). This suggests that the dual compartment model used induce a more efficient differentiation, driving cell towards mature and specialized phenotype. The morphological results described above are consistent with Marrazzo et al. (2016) that reported the acquisition of an elongated columnar morphology in tracheobronchial epithelial cells co-cultured with fibroblasts onto Alvetex® systems. Notably, when the same epithelial cells were grown onto Transwell® membranes, they maintained a flat undifferentiated shape with a very reduced similarity to the tracheal cells *in vivo* (Marrazzo et al., 2016).

The histological data obtained in our experiments are also supported by molecular evidence that show higher transcription levels of VIM, THY1, KRT5, KRT14, KRT18 and TJP1 genes in the 3D Alvetex platform compared to those detected in hDF and hTEpC cultured as monolayer onto 2D standard plastic dishes (Fig. 2 D). It is interesting to note that a comparable expression pattern was previously described by other Authors that reported the generation of a human 3D epithelial model constituted by fibroblasts and tracheobronchial epithelial cells co-cultured onto Alvetex® inserts (Marrazzo et al., 2016).

2.2. *I3C effect on viral egression-related genes in intestinal and tracheal 3D models*

Viral egression is an important step of the viral life cycle and allows viruses from host cells to spread to other cells. During this stage, new

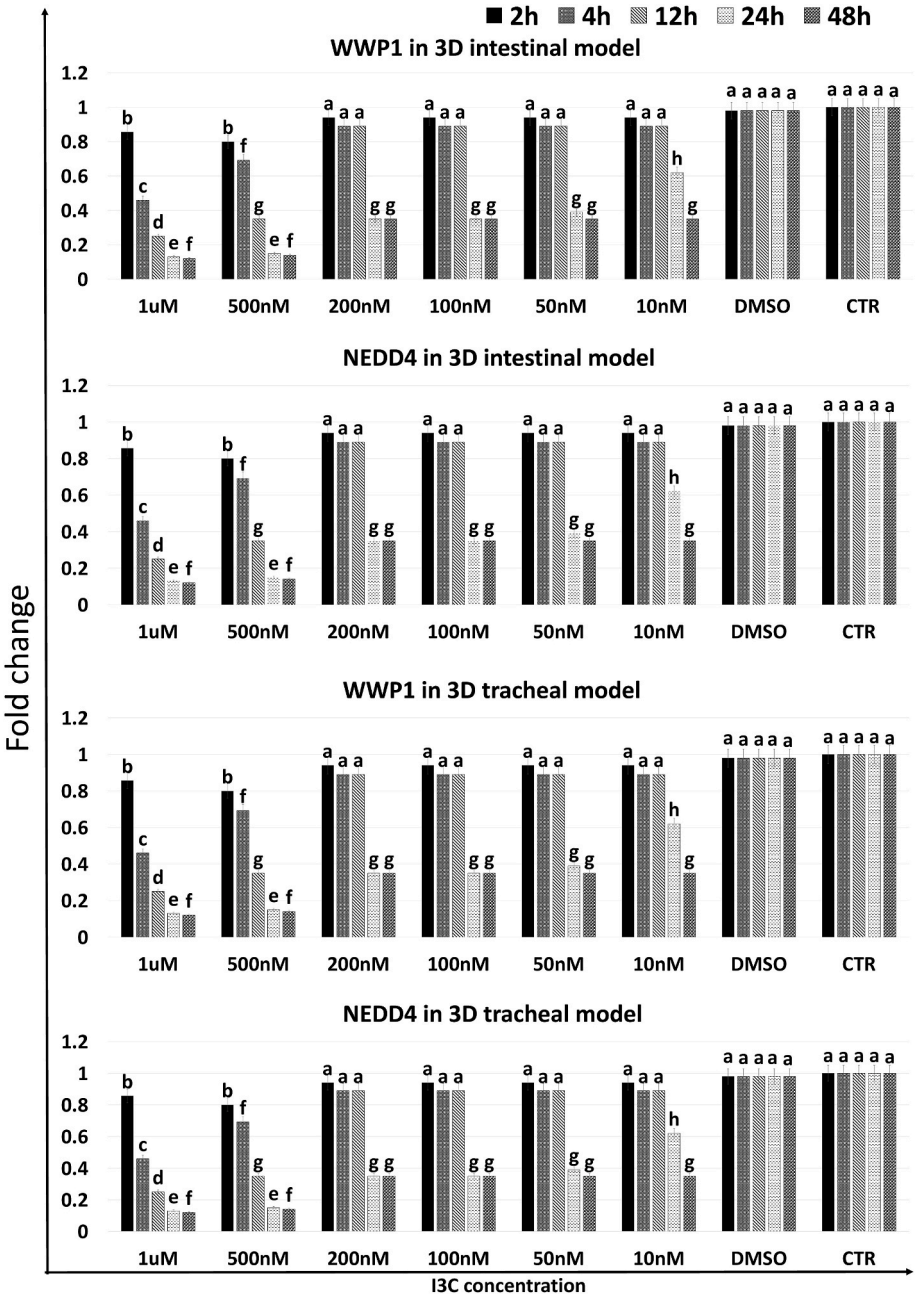

Fig. 3. *Gene expression levels of WWP1 and NEDD4 genes in intestinal and tracheal 3D models exposed to I3C with different concentrations and times of incubation.* Data are expressed as the mean. Error bars represent the standard error of the mean (SEM). Different superscripts indicate $p < 0.05$.

viral particles are assembled and subsequently released by endocytotic processes (Ghosh et al., 2020; Knoops et al., 2008; Snijder et al., 2020; Zhang and Zhang, 2021) under the influence of the HECT-E3 ligases. In particular, it has been demonstrated that the HECT family members, not only physically interact with viral proteins to regulate the release of mature viral particles, by high jacking the endosomal sorting complexes required for transport (ESCRT) machinery (Scheffner and Kumar, 2014; Schmidt and Teis, 2012; Vietri et al., 2019), but also influence endocytosis through ubiquitination (Shih et al., 2000). Among the different HECT family members, WWP1 and NEDD4 have been identified as important actors that interact with and ubiquitylate the SARS-CoV-2 Spike protein (Novelli et al., 2021), thus expanding and confirming previous reports describing their involvement in the cell egression phase of deadly RNA viruses, such as Ebola through direct interaction of its VP40 Protein (Han et al., 2017).

In the present manuscript, we hypothesize that I3C, a natural NEDD4 and WWP1 inhibitor from *Brassicaceae*, may display antiviral effects, impeding viral egression. We expose the 3D intestinal and tracheal models, described in the previous paragraphs, to different I3C concentrations, ranging from 1 μM to 10 nM, for 2, 4, 12, 24, and 48 h. The results obtained demonstrate that in both 3D models used NEDD4 and WWP1 gene expression levels are significantly decreased after 2 h of treatment with 1 μM and 500 nM concentrations (Fig. 3). Lower doses comprised between 200 and 10 nM do not affect the transcription values of these genes, compared to CTR and vehicle (DMSO), after 2-, 4- and 12-h exposure (Fig. 3). However, a significant downregulation of NEDD4 and WWP1 genes is detected when the 3D *in vitro* models are incubated for 24 and 48 h regardless to the I3C concentrations used (Fig. 3). This is consistent with previous studies describing I3C as a natural organic compound with pleiotropic effects and regulatory actions on the transcription of multiple genes and several signaling pathways (Karimabad et al., 2019; Li et al., 2003; Wang et al., 2012; Weng et al., 2007). More in detail, a whole transcriptional, analysis carried out on cells treated with I3C, showed a 2-fold change in expression of 685 genes, which were down-regulated (Li et al., 2003)That study also indicated, among the several pathways affected, a direct impact on EGF receptor and JAK-STAT cascade transcription levels (Li et al., 2003). Notably, these two pathways play a key role in NEDD4 and WWP1 gene regulation, respectively, thus suggesting that the I3C inhibitory effects described in the present manuscript may derive from EGF receptor and JAK-STAT cascade down-regulation. In particular, we hypothesize that NEDD4 diminished expression may results from I3C inhibitory effect on the EGF receptor, while WWP1 gene transcription down-regulation may be related to JAK-STAT suppression.

Overall, the data obtained indicate that the phytochemical is able to induce a direct dose- and time-dependent inhibition of the main HECT family members involved in virus replication, both in porcine and human species. While no previous information was available for the former, our observations are consistent with recent findings by Novelli et al. (2021), who reported I3C efficacy in mediating SARS-CoV- 2 antiviral effect in the human. It is however important to note that the I3C effective concentrations in that work were higher than those demonstrated in the experiments here described. We have no clear explanation for this discrepancy, but we hypothesize that a different sensibility to I3C of the models used may be a possible reason. As a side note, it is evident that low concentrations of the phytochemical shown to be active in this study better correlate I3C protective/preventing effects with basic nutrition needs.

3. Conclusions

Our findings suggest a protective effect of I3C against the early stages of coronaviridae infections. In particular, this phytochemical found in *Brassicaceae* is able to counteract the ubiquitination of the viral matrix proteins in two different *in vitro* models of tracheal and intestinal tissues. I3C effects on transcription levels of the main HECT family members, that control virus life cycle, pave the way to the possible therapeutic use of natural compounds in reducing viral egression and preventing the clinical severity of future pandemics.

4. Experimental

All reagents were purchased from Sigma-Aldrich unless otherwise indicated.

4.1. Ethic statement

Intestinal porcine epithelial cell line-J2 (IPEC-J2) and human tracheal epithelial cells (hTEpC) were obtained from DSMZ (Braunschweig, Germany) and PromoCell (Heidelberg, Germany), respectively. Porcine dermal fibroblasts (pDF) were obtained from fresh skin biopsies collected at the local abattoir from adult animals. Human dermal fibroblasts (hDF) were isolated from dermal biopsies of adult healthy individual, after the Ethical Committee of the Ospedale Maggiore Policlinico - Milano approval and written informed consent. All experiments were performed in accordance with the approved guidelines.

4.2. IPEC-J2 cell growth and maintenance onto standard plastic dishes

IPEC-J2 cells were cultured in Dulbecco's Modified Eagle Medium: Nutrient Mixture F12 (DMEM F12, Thermo-Fisher-Scientific) supplemented with 5% Foetal Bovine Serum (FBS, Thermo-Fisher-Scientific), 2 mM glutamine and antibiotics. Cells were passaged twice a week at 1:6 ratio and maintained in 5% CO_2 at 37 °C.

4.3. hTEpC growth and maintenance onto standard plastic dishes

hTEpC were cultured in Bronchia/Trachea Epithelial Cell Growth Medium (Cell applications) supplemented with 0.05 μM retinoic acid (Cell applications) in 5% CO_2 at 37 °C. When cells reached 70% of confluency, they were passaged at 1:3 ratio and maintained in 5% CO_2 at 37 °C.

4.4. pDF isolation, growth, and maintenance onto standard plastic dishes

Porcine skin explants were cut in small fragments of approximately 2 mm^3, placed onto 0.1% porcine gelatin pre-coated Petri dish (Sarstedt) and cultured in DMEM (Thermo-Fisher-Scientific), supplemented with 20% FBS, 2 mM glutamine and antibiotics. After 6 days of culture, fragments were carefully removed and fibroblasts were maintained in the medium described above supplemented with 10% FBS, grown in 5% CO2 at 37 °C, and passaged twice a week at 1:3 ratio.

4.5. hDF isolation, growth, and maintenance onto standard plastic dishes

Human dermal fragments of approximately 2 mm^3 were placed onto 0.1% gelatin pre-coated Petri dish (Sarstedt) and cultured in Dulbecco's modified Eagle's medium (DMEM, Thermo-Fisher-Scientific) supplemented with 20% Foetal Bovine Serum (FBS, Thermo-Fisher-Scientific), 2 mM glutamine and antibiotics. Cells started to grow out of the fragments after 6 days of culture. Skin pieces were carefully removed, and fibroblasts were maintained in the medium described above supplemented with 10% FBS. Cells were passaged twice a week at 1:3 ratio and grown in 5% CO_2 at 37 °C.

4.6. Porcine intestinal 3D culture model assembly

12-well Alvetex® Scaffold inserts (Reprocell Europe, United Kingdom) were prepared according to manufacturer's instructions. 0.5 × 10^6 pDF were seeded onto inserts at days 0, 7 and 9 of culture and grown in DMEM supplemented with 20% FBS, 2 mM glutamine, 5 ng/mL TGF β1 (Thermo-Fisher-Scientific) and 100 μg/mL ascorbic acid, and

antibiotics in 5% CO_2 at 37 °C for 14 days. Medium was refreshed twice a week.

On day 14, 0.4 × 10^6 IPEC-J2 cells were layered on the stromal compartment and maintained in DMEM F12 supplemented with 5% FBS, 2 mM glutamine and antibiotics for 21 days. Cultures were maintained in 5% CO_2 at 37 °C and medium was refreshed twice a week.

4.7. Human tracheal 3D culture model assembly

The stromal compartment was generated using 12-well Alvetex® Scaffold inserts as described above. After 14 days of culture, hTEpC were seeded onto 3D fibroblast cultures at a density of 0.4 × 10^6 cells/insert and grown in complete Bronchia/Trachea Epithelial Cell Growth Medium for 6 days. From day 7 onward, cells were further differentiated using Bronchia/Trachea Epithelial Cell Differentiation Medium (Cell applications) and cultured until day 28 in 5% CO_2 at 37 °C.

4.8. I3C exposure of intestinal and tracheal 3D models

Porcine intestinal and Human tracheal 3D models were exposed to different concentrations of synthetic I3C (Sigma-Aldrich, #I7256): 1 μM, 500 nM, 200 nM, 100 nM, 50 nM and 10 nM and incubated for 2, 4, 12, 24 and 48 h. I3C stock solution was prepared by dissolving 1.47 mg of powder in 1 mL of DMSO. Subsequently, the different working solutions were prepared. DMSO was used as vehicle. Culture medium was used as control (CTR).

4.9. Gene expression analysis

RNA was extracted from the samples using TaqManGene Expression Cells-to-CT kit (Thermo-Fisher-Scientific), following the manufacturer's instruction. DNase I was added in lysis solution at 1:100 concentration. Quantitative Real-Time PCR was performed using predesigned gene-specific primers and probe sets from TaqManGene Expression Assays (Table 1) with the CFX96 Real-Time PCR detection system (Bio-Rad Laboratories). Target gene quantification was carried out with CFX Manager software (Bio-Rad Laboratories) using GAPDH and ACTB as internal reference genes and here reported with the highest expression set to 1 and the other relative to this.

4.10. Histological analysis

At the end of culture, tracheal and intestinal 3D models were fixed in 4% PFA for 24 h, dehydrated through a series of ethanol, incubated in Histoclear (Bio-optica) and embedded in paraffin. 5–7 μm thick sections were cut, dewaxed, re-hydrated, and stained with haematoxylin/eosin (HE). Samples were analyzed using Leica DMR microscope (Leica Microsystems).

4.11. Functional evaluation of the intestinal 3D model

Intestinal barrier TEER was measured using an EVOM2 Epithelial Voltmeter with STX3 electrode (World Precision Instrument). The electrode was equilibrated according to the manufacturer's instruction. The electrode was insert in the 3 sides of each insert and the final TEER value was determined as follows:

TEER (Ohm x cm^2) = (TEER average sample insert – TEER average blank insert) x Area $cm.^2$

4.12. Statistical analysis

Statistical analysis was performed using two-way ANOVA (SPSS 19.1; IBM). Data were presented as mean ± standard deviation (SD). Differences of $p \leq 0.05$ were considered significant and were indicated with different superscripts.

Table 1
List of primers used for quantitative PCR analysis.

GENE	DESCRIPTION	SPECIES	Cat.N.
ACTB	Actin beta	Porcine	Ss03376563_uH
GAPDH	Glyceraldehyde-3-phosphate dehydrogenase	Porcine	Ss03374854_g1
VIL1	Villin 1	Porcine	Ss06886976_m1
ZO1 (TJP1)	Tight junction protein 1	Porcine	Ss03373514_m1
OCLN	Occludin	Porcine	Ss03377507_u1
CLDN1	Claudin 1	Porcine	Ss03375708_u1
WWP1	E3 ubiquitin ligase WWP1	Porcine	Ss06879119_s1
NEDD4	E3 ubiquitin ligase NEDD4	Porcine	Ss06866232_m1
ACTB	Actin beta	Human	Hs01060665_g1
GAPDH	Glyceraldehyde-3-phosphate dehydrogenase	Human	Hs02786624_g1
KRT5	Cytokeratin 5	Human	Hs00934200_g1
KRT14	Cytokeratin 14	Human	Hs01588587_g1
KRT18	Cytokeratin 18	Human	Hs02827483_g1
ZO1 (TPJ1)	Tight Junction protein 1	Human	Hs00543810_g1
WWP1	E3 ubiquitin ligase WWP1	Human	Hs00366927_m1
NEDD4	E3 ubiquitin ligase NEDD4	Human	Hs00406454_m1

Declaration of competing interest

The authors declare that they have no known competing financial interests or personal relationships that could have appeared to influence the work reported in this paper.

Data availability

Data will be made available on request.

Acknowledgments

This research was funded by Carraresi Foundation, PSR2021, PSR2022, HORIZON-WIDERA-2021 project n#101079349 (OH-Boost) and it is part of the project "MIND FoodS HUB (Milano Innovation District Food System Hub): Innovative concept for the eco-intensification of agricultural production and for the promotion of dietary patterns for human health and longevity through the creation in MIND of a digital Food System Hub", cofunded by PORFESR 2014–2020_BANDO Call HUB Ricerca e Innovazione, Regione Lombardia. Authors are members of the Trans-COST Actions Task-Force on Covid-19. TB is member of the COST Action CA20140, CorEuStem.

References

Antunes, F., Andrade, F., Araújo, F., Ferreira, D., Sarmento, B., 2013. Establishment of a triple co-culture in vitro cell models to study intestinal absorption of peptide drugs. Eur. J. Pharm. Biopharm. 83, 427–435. https://doi.org/10.1016/J.EJPB.2012.10.003.

Béduneau, A., Tempesta, C., Fimbel, S., Pellequer, Y., Jannin, V., Demarne, F., Lamprecht, A., 2014. A tunable Caco-2/HT29-MTX co-culture model mimicking variable permeabilities of the human intestine obtained by an original seeding procedure. Eur. J. Pharm. Biopharm. 87, 290–298. https://doi.org/10.1016/J.EJPB.2014.03.017.

Bernardo, M.E., Fibbe, W.E., 2013. Mesenchymal stromal cells: sensors and switchers of inflammation. Cell Stem Cell 13, 392–402. https://doi.org/10.1016/j.stem.2013.09.006.

Costello, L., Darling, N., Freer, M., Bradbury, S., Mobbs, C., Przyborski, S., 2021. Use of porous polystyrene scaffolds to bioengineer human epithelial tissues in vitro. Methods Mol. Biol. 2273, 279–296. https://doi.org/10.1007/978-1-0716-1246-0_20.

Darling, N.J., Mobbs, C.L., González-Hau, A.L., Freer, M., Przyborski, S., 2020. Bioengineering novel in vitro Co-culture models that represent the human intestinal mucosa with improved caco-2 structure and barrier function. Front. Bioeng. Biotechnol. 8 https://doi.org/10.3389/FBIOE.2020.00992.

Gavriatopoulou, M., Korompoki, E., Fotiou, D., Ntanasis-Stathopoulos, I., Psaltopoulou, T., Kastritis, E., Terpos, E., Dimopoulos, M.A., 2020. Organ-specific manifestations of COVID-19 infection. Clin. Exp. Med. 20, 493. https://doi.org/10.1007/S10238-020-00648-X.

Ghosh, R., Dubey, M.J., Chatterjee, S., Dubey, S., 2020. Impact of COVID-19 on children: special focus on the psychosocial aspect. Minerva Pediatr. 72, 226–235. https://doi.org/10.23736/S0026-4946.20.05887-9.

Halttunen, T., Marttinen, A., Rantala, I., Kainulainen, H., Maki, M., 1996. Fibroblasts and transforming growth factor β induce organization and differentiation of T84 human epithelial cells. Gastroenterology 111, 1252–1262. https://doi.org/10.1053/gast.1996.v111.pm8898639.

Han, Z., Sagum, C.A., Takizawa, F., Ruthel, G., Berry, C.T., Kong, J., Sunyer, J.O., Freedman, B.D., Bedford, M.T., Sidhu, S.S., Sudol, M., Harty, R.N., 2017. Ubiquitin ligase WWP1 interacts with Ebola virus VP40 to regulate egress. J. Virol. 91 https://doi.org/10.1128/JVI.00812-17.

Hausmann, C., Zoschke, C., Wolff, C., Darvin, M.E., Sochorová, M., Kováčik, A., Wanjiku, B., Schumacher, F., Tigges, J., Kleuser, B., Lademann, J., Fritsche, E., Vávrová, K., Ma, N., Schäfer-Korting, M., 2019. Fibroblast origin shapes tissue homeostasis, epidermal differentiation, and drug uptake. Scientific Reports 2019 9 (1 9), 1–10. https://doi.org/10.1038/s41598-019-39770-6.

Karimabad, M.N., Mahmoodi, M., Jafarzadeh, A., Darekordi, A., Hajizadeh, M.R., Hassanshahi, G., 2019. Molecular targets, anti-cancer properties and potency of synthetic indole-3-carbinol derivatives. Mini Rev. Med. Chem. 19, 540–554. https://doi.org/10.2174/1389557518666181116120145.

Kedinger, M., Duluc, I., Fritsch, C., Lorentz, O., Plateroti, M., Freund, J.N., 1998. Intestinal epithelial-mesenchymal cell interactions. Ann. N. Y. Acad. Sci. 859, 1–17. https://doi.org/10.1111/J.1749-6632.1998.TB11107.X.

Kim, J.H., Lee, B.W., Schroeder, F.C., Jander, G., 2008. Identification of indole glucosinolate breakdown products with antifeedant effects on Myzus persicae (green peach aphid). Plant J. 54, 1015–1026. https://doi.org/10.1111/J.1365-313X.2008.03476.X.

Knoops, K., Kikkert, M., van den Worm, S.H.E., Zevenhoven-Dobbe, J.C., van der Meer, Y., Koster, A.J., Mommaas, A.M., Snijder, E.J., 2008. SARS-coronavirus replication is supported by a reticulovesicular network of modified endoplasmic reticulum. PLoS Biol. 6, e226. https://doi.org/10.1371/JOURNAL.PBIO.0060226.

Korpos, E., Wu, C., Song, J., Hallmann, R., Sorokin, L., 2010. Role of the extracellular matrix in lymphocyte migration. Cell Tissue Res. 339, 47–57. https://doi.org/10.1007/S00441-009-0853-3/FIGURES/3.

Li, Y., Li, X., Sarkar, F.H., 2003. Gene expression profiles of I3C- and DIM-treated PC3 human prostate cancer cells determined by cDNA microarray analysis. J. Nutr. 133, 1011–1019. https://doi.org/10.1093/JN/133.4.1011.

Marrazzo, P., Maccari, S., Taddei, A., Bevan, L., Telford, J., Soriani, M., Pezzicoli, A., 2016. 3D reconstruction of the human airway mucosa in vitro as an experimental model to study NTHi infections. PLoS One 11, e0153985. https://doi.org/10.1371/JOURNAL.PONE.0153985.

Matsusaki, M., Hikimoto, D., Nishiguchi, A., Kadowaki, K., Ohura, K., Imai, T., Akash, M., 2015. 3D-fibroblast tissues constructed by a cell-coat technology enhance tight-junction formation of human colon epithelial cells. Biochem. Biophys. Res. Commun. 457, 363–369. https://doi.org/10.1016/J.BBRC.2014.12.118.

Novelli, G., Liu, J., Biancolella, M., Alonzi, T., Novelli, A., Patten, J.J., Cocciadiferro, D., Agolini, E., Colona, V.L., Rizzacasa, B., Giannini, R., Bigio, B., Goletti, D., Capobianchi, M.R., Grelli, S., Mann, J., McKee, T.D., Cheng, K., Amanat, F., Krammer, F., Guarracino, A., Pepe, G., Tomino, C., Tandjaoui-Lambiotte, Y., Uzunhan, Y., Tubiana, S., Ghosn, J., Notarangelo, L.D., Su, H.C., Abel, L., Cobat, A., Elhanan, G., Grzymski, J.J., Latini, A., Sidhu, S.S., Jain, S., Davey, R.A., Casanova, J. L., Wei, W., Pandolfi, P.P., 2021. Inhibition of HECT E3 ligases as potential therapy for COVID-19. Cell Death & Disease 2021 12 (4 12), 1–18. https://doi.org/10.1038/s41419-021-03513-1.

Pereira, C., Araújo, F., Barrias, C.C., Granja, P.L., Sarmento, B., 2015. Dissecting stromal-epithelial interactions in a 3D in vitro cellularized intestinal model for permeability studies. Biomaterials 56, 36–45. https://doi.org/10.1016/J.BIOMATERIALS.2015.03.054.

Pi, G., Song, W., Wu, Z., Li, Y., Yang, H., 2022. Comparison of expression profiles between undifferentiated and differentiated porcine IPEC-J2 cells. Porcine Health Manag 8, 1–12. https://doi.org/10.1186/S40813-022-00247-0/FIGURES/10.

Richter, J.F., Pieper, R., Zakrzewski, S.S., Günzel, D., Schulzke, J.D., van Kessel, A.G., 2014. Diets high in fermentable protein and fibre alter tight junction protein composition with minor effects on barrier function in piglet colon. Br. J. Nutr. 111, 1040–1049. https://doi.org/10.1017/S0007114513003498.

Scheffner, M., Kumar, S., 2014. Mammalian HECT ubiquitin-protein ligases: biological and pathophysiological aspects. Biochim. Biophys. Acta Mol. Cell Res. 1843, 61–74. https://doi.org/10.1016/J.BBAMCR.2013.03.024.

Schmidt, O., Teis, D., 2012. The ESCRT machinery. Curr. Biol. 22, R116–R120. https://doi.org/10.1016/j.cub.2012.01.028.

Schweinlin, M., Wilhelm, S., Schwedhelm, I., Hansmann, J., Rietscher, R., Jurowich, C., Walles, H., Metzger, M., 2016. Development of an Advanced Primary Human in Vitro Model of the Small Intestine, pp. 873–883. https://doi.org/10.1089/TEN.TEC.2016.0101. https://home.liebertpub.com/tec 22.

Shih, S.C., Sloper-Mould, K.E., Hicke, L., 2000. Monoubiquitin carries a novel internalization signal that is appended to activated receptors. EMBO J. 19, 187–198. https://doi.org/10.1093/EMBOJ/19.2.187.

Singh, A.A., Patil, M.P., Kang, M.J., Niyonizigiye, I., Kim, G. do, 2021a. Biomedical application of Indole-3-carbinol: a mini-review. Phytochem. Lett. 41, 49–54. https://doi.org/10.1016/J.PHYTOL.2020.09.024.

Singh, A.A., Patil, M.P., Kang, M.J., Niyonizigiye, I., Kim, G. do, 2021b. Biomedical application of Indole-3-carbinol: a mini-review. Phytochem. Lett. 41, 49–54. https://doi.org/10.1016/J.PHYTOL.2020.09.024.

Snijder, E.J., Limpens, R.W.A.L., de Wilde, A.H., de Jong, A.W.M., Zevenhoven-Dobbe, J. C., Maier, H.J., Faas, F.F.G.A., Koster, A.J., Bárcena, M., 2020. A unifying structural and functional model of the coronavirus replication organelle: tracking down RNA synthesis. PLoS Biol. 18, e3000715 https://doi.org/10.1371/JOURNAL.PBIO.3000715.

Sung, W.S., Lee, D.G., 2007. In vitro antimicrobial activity and the mode of action of indole-3-carbinol against human pathogenic microorganisms. Biol. Pharm. Bull. 30, 1865–1869. https://doi.org/10.1248/BPB.30.1865.

Takada, Y., Andreeff, M., Aggarwal, B.B., 2005. Indole-3-carbinol suppresses NF-kappaB and IkappaBalpha kinase activation, causing inhibition of expression of NF-kappaB-regulated antiapoptotic and metastatic gene products and enhancement of apoptosis in myeloid and leukemia cells. Blood 106, 641–649. https://doi.org/10.1182/BLOOD-2004-12-4589.

Takenaka, T., Harada, N., Kuze, J., Chiba, M., Iwao, T., Matsunaga, T., 2014. Human small intestinal epithelial cells differentiated from adult intestinal stem cells as a novel system for predicting oral drug absorption in humans. Drug Metabol. Dispos. 42, 1947–1954. https://doi.org/10.1124/DMD.114.059493.

Troisi, J., Venutolo, G., Tanyà, M.P., Carri, M.D., Landolfi, A., Fasano, A., 2021. COVID-19 and the gastrointestinal tract: source of infection or merely a target of the inflammatory process following SARS-CoV-2 infection? World J. Gastroenterol. 27, 1406. https://doi.org/10.3748/WJG.V27.I14.1406.

Vergauwen, H., 2015. The IPEC-J2 cell line. The Impact of Food Bioactives on Health: In Vitro and Ex Vivo Models 125–134. https://doi.org/10.1007/978-3-319-16104-4_12.

Vietri, M., Radulovic, M., Stenmark, H., 2019. The many functions of ESCRTs. Nature Reviews Molecular Cell Biology 2019 21 (1 21), 25–42. https://doi.org/10.1038/s41580-019-0177-4.

Wang, T.T.Y., Schoene, N.W., Milner, J.A., Kim, Y.S., 2012. Broccoli-derived phytochemicals indole-3-carbinol and 3,3′-diindolylmethane exerts concentration-dependent pleiotropic effects on prostate cancer cells: comparison with other cancer preventive phytochemicals. Mol. Carcinog. 51, 244–256. https://doi.org/10.1002/MC.20774.

Weng, J.R., Tsai, C.H., Kulp, S.K., Chen, C.S., 2008. Indole-3-carbinol as a chemopreventive and anti-cancer agent. Cancer Lett. 262, 153–163. https://doi.org/10.1016/J.CANLET.2008.01.033.

Weng, J.R., Tsai, C.H., Kulp, S.K., Wang, D., Lin, C.H., Yang, H.C., Ma, Y., Sargeant, A., Chiu, C.F., Tsai, M.H., Chen, C.S., 2007. A potent indole-3-carbinol derived antitumor agent with pleiotropic effects on multiple signaling pathways in prostate cancer cells. Cancer Res. 67, 7815–7824. https://doi.org/10.1158/0008-5472.CAN-07-0794.

Zakrzewski, S.S., Richter, J.F., Krug, S.M., Jebautzke, B., Lee, I.F.M., Rieger, J., Sachtleben, M., Bondzio, A., Schulzke, J.D., Fromm, M., Günze, D., 2013. Improved cell line IPEC-J2, characterized as a model for porcine jejunal epithelium. PLoS One 8. https://doi.org/10.1371/JOURNAL.PONE.0079643.

Zhang, Hui, Zhang, Hong, 2021. Entry, egress and vertical transmission of SARS-CoV-2. J. Mol. Cell Biol. 13, 168–174. https://doi.org/10.1093/JMCB/MJAB013.

Zhao, Y., Wang, J., Liu, Y., Miao, H., Cai, C., Shao, Z., Guo, R., Sun, B., Jia, C., Zhang, L., Gigolashvili, T., Wang, Q., 2015. Classic myrosinase-dependent degradation of indole glucosinolate attenuates fumonisin B1-induced programmed cell death in Arabidopsis. Plant J. 81, 920–933. https://doi.org/10.1111/TPJ.12778.